Analyst

Zn
Cd
Pb
Fe Ni Cu
E vs (Ag)/V

ROYAL SOCIETY
OF CHEMISTRY

PAPER
Wendell K. T. Coltro *et al.*
Plug-and-play assembly of paper-based colorimetric and
electrochemical devices for multiplexed detection of metals

PAPER

Check for updates

Plug-and-play assembly of paper-based colorimetric and electrochemical devices for multiplexed detection of metals†

Habdias A. Silva-Neto, [a] Thiago M. G. Cardoso,[a] Catherine J. McMahon,[b] Lívia F. Sgobbi,[a] Charles S. Henry [b] and Wendell K. T. Coltro [a,c]

Heavy metals are the main pollutants present in aquatic environments and their presence in human organisms can lead to many different diseases. While many methods exist for analysis, colorimetric and electrochemistry are particularly attractive for on-site analysis and their integration on a single platform can improve multiplexed metals analysis. This report describes for the first time a "plug-and-play" (PnP) assembly for coupling a microfluidic paper-based device (µPAD) and a screen-printed electrochemical paper-based device (ePAD) using a vertical and reversible foldable mechanism for multiplexed detection of Fe, Ni, Cu, Zn, Cd and Pb in river water samples. The integration strategy was based on a reversible assembly, allowing the insertion of a pretreatment zone to minimize potential chemical interfering agents and providing a better control of the aspirated sample volume as well as to a lower sample evaporation rate. In comparison with lateral flow and electrochemical assays performed using independent devices, the integrated prototype proved that the reversible coupling mechanism does not interfere on the analytical performance (95% confidence interval). The limit of detection (LOD) values calculated for metals determined varied from 0.1 to 0.3 mg L^{-1} (colorimetric) and from 0.9 to 10.5 µg L^{-1} (electrochemical). When compared to other integrated devices based on horizontal designs, the use of a foldable coupling mechanism offered linear response in a lower concentration range and better LOD values for Fe, Ni and Cu. The proposed method successfully measured heavy metals in river water samples with concentrations ranging from 16 to 786 µg L^{-1}, with recovery studies ranging from 76 to 121%. The new method also showed good correlation with conventional atomic absorption spectroscopic methods (95% significance level). Thus, the integration of µPADs and ePADs by a vertical folding mechanism was efficient for multiplexed heavy metal analysis and could be exploited for environmental monitoring.

1. Introduction

The implementation of strict environmental regulations has increased the demand for rapid, reliable and accurate analytical methods that are also fieldable and user-friendly. Continuous monitoring of environmentally relevant compounds like heavy metals is of specific concern.[1–3] Traditional analysis of heavy metals centers around atomic spectroscopy techniques, including atomic absorption spectroscopy, induc-

tively coupled plasma mass spectrometry and inductively coupled plasma atomic emission spectrometry, which employ expensive and bulky instruments, make use of large volumes of sample and reagents, generate considerable amount of waste, require long analysis time and need intense technical training.[4–6] For these reasons, the development of simpler, greener, and faster methodologies for monitoring environmental pollutants is encouraged.[3–5]

Paper-based platforms have become widely known for the development of analytical devices.[4–9] Since their conception, microfluidic paper-based analytical devices (µPADs) and electrochemical paper-based analytical devices (ePADs) have received noticeable attention for applications in different fields including the analysis of metals.[10–13] Colorimetry and electrochemistry are two of the most common detection modes used on paper-based devices.[14,15] While colorimetric detection can be performed using digital image analysis or dis-

[a]Instituto de Química, Universidade Federal de Goiás, 74690-900 Goiânia, GO, Brazil. E-mail: wendell@ufg.br; Fax: +55 62 3521 1127
[b]Department of Chemistry, Colorado State University, 80523 Fort Collins, CO, USA
[c]Instituto Nacional de Ciência e Tecnologia de Bioanalítica, 13083-861 Campinas, SP, Brazil
†Electronic supplementary information (ESI) available. See DOI: 10.1039/d1an00176k

tance-based methods,[16,17] various electroanalytical methods including amperometry, voltammetry and contactless conductometry have been also coupled to this platform.[16–24]

μPADs and ePADs have emerged as powerful alternative tools for environmental applications.[25–30] There are several reports that either use μPADs for colorimetric detection or ePADs for electrochemical detection of select heavy metals including iron, copper, nickel, mercury, lead, chromium, zinc and cadmium.[9,26,31] Colorimetric assays offer instrumental simplicity with chemical information based on the color development,[32] while electrochemical measurements provide better sensitivity and selectivity, especially when stripping techniques are employed.[28,33,34] The inherent advantages of each detection mode can be combined into a single integrated device, resulting in a powerful and cost effective analytical tool for rapid and multiplexed analysis exploiting the same sample aliquot.[26,35]

The integration of dual colorimetric and electrochemical approaches on paper-based microfluidic platforms has been reported by a few research groups. The pioneering study was described by Apilux et al.,[36] who successfully demonstrated the coupling of electrochemical and colorimetric measurements on a μPAD to simultaneously detect Au(III) in the presence of Fe(III), as interfering agent, in industrial waste solutions. Rattanarat et al.[26] developed a multilayer sensor for dual colorimetric and electrochemical analysis of metals. The device consisted of screen-printed electrodes on a polyester film surface with wax-printed μPADs that were folded irreversibly over the electrodes using double-sided adhesive tape. Colorimetric and electrochemical analysis of Fe, Ni, Cr, Cu, Pb and Cd were demonstrated in particulate matter. Silva et al.[35] described the integration of a colorimetric detection mechanism and an electrochemical sample pretreatment. The authors integrated wax-printed μPADs with commercially available screen-printed electrodes for the detection of procaine based on a single folding step. The adopted strategy successfully eliminated the interference of benzocaine on the colorimetric detection of procaine in seized cocaine samples. Chaiyo et al.[37] presented an efficient coupling of boron-doped diamond electrode and μPAD using double-sided adhesive tape. The dual system was explored for the simultaneous electrochemical detection of Cd and Pb and colorimetric measurements of Cu in environmental and food samples.

While reports have successfully demonstrated the planar integration of dual colorimetric and electrochemical detectors on simple and low-cost analytical platforms, the fabrication of integrated electrochemical and microfluidic structures entirely on paper has been limited. One of the main challenges involved in the integration of both paper-based colorimetric and electrochemical devices is sample evaporation and loss. Here, we propose for the first time a plug-and-play (PnP) assembly for allowing the reversible coupling of μPAD and ePAD. The proof-of-concept was successfully demonstrated through simultaneous analysis of Zn, Cd, Pb, Fe, Ni and Cu in river water samples. Both colorimetric and electro-

chemical devices were developed on paper substrates and fixed on a flexible polymer substrate with ability to be folded and unfolded through a PnP strategy. To ensure the properly connection between ePAD and potentiostat, an external holder was constructed by 3D printing to make the instrumental handling simple and reproducible. In comparison with the planar integration, the PnP strategy has demonstrated ability to minimize the problems commonly observed on paper-based devices coupled with dual detection. The analytical performance of the proposed device, including the sensitivity, selectivity, accuracy and reliability was thoroughly investigated.

2. Experimental

2.1 Chemicals and materials

Copper sulfate pentahydrate, ammonium iron(II) sulfate hexahydrate, nickel nitrate hexahydrate, zinc nitrate hexahydrate, cadmium nitrate tetrahydrate, lead nitrate, bismuth(III) nitrate pentahydrate, ammonium chloride, sodium fluoride, sodium phosphate dibasic, sodium phosphate monobasic, potassium chloride, potassium hexacyanoferrate(II) trihydrate, potassium hexacyanoferrate(III), sodium acetate, acetic acid, hydroxylamine hydrochloride, bathocuproine, polyethylene glycol 400 (PEG 400), dimethylglyoxime, methacrylic acid, bathophenanthroline, barium nitrate, antimony(III) chloride, aluminum sulfate octadecahydrate, manganese sulfate monohydrate and, potassium dichromate were purchased from Sigma-Aldrich (Saint Louis, MO, USA) and used as received. Stock and standard solutions were prepared using ultrapure water processed through a water purification system (Direct-Q®3 model, Millipore, Darmstadt, Germany) with resistivity equal to 18.2 MΩ cm.

Whatman® grade 1 chromatography paper (200 mm × 200 mm, thickness: 0.18 mm), Whatman® grade 42 quantitative paper (200 mm × 200 mm, porous size: 2.5 μm) and multiwalled carbon nanotubes (MWCNT) (code 724769, OD: 6–9 nm, length: 5 μm) were received from Sigma-Aldrich (Saint Louis, MO, USA). JP40 quantitative paper (grade 40, ∅ = 125 mm, porous size: 25 μm) was purchased from J. Prolab (São José dos Pinhais, PR, Brazil). Vegetal paper (210 mm × 297 mm, weight = 180 g m⁻²), Vitral varnish (alternative binder), and graphite powder were purchased from Filiperson (Rio de Janeiro, RJ, Brazil), Acrilex (São Bernardo do Campo, SP, Brazil) and Synth (Diadema, SP, Brazil), respectively. The universal serial bus cable (USB 3.0) with integrated gold film was acquired from Tronsmart (Shenzhen, China). Thermal laminating pouches (thickness: 250 μm), also named as thermosensitive polyester films, were ordered from Yidu Group Co., Ltd (Hsi-Chih, Taipei, Taiwan).

2.2 Fabrication of microfluidic and electrochemical paper-based analytical devices

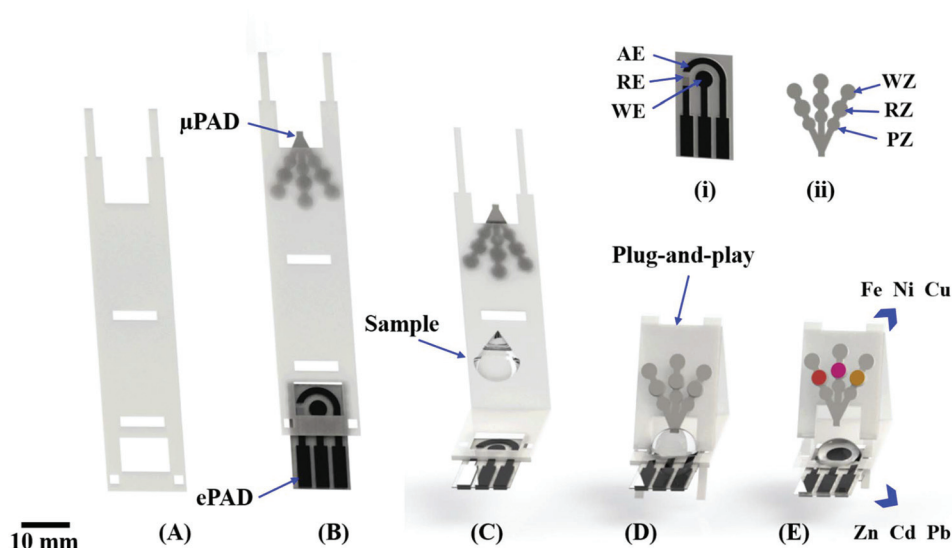The fabrication of the μPADs was done on chromatography paper (grade 1). The layout of the μPAD was drawn in the

Fig. 1 Scheme showing the coupling of µPAD and ePAD for dual colorimetric/electrochemical detection of metals. Image (A) displays a thermosensitive polyester film used to fix (B) both µPAD and ePAD at the extremities; images (C) and (D) denote the sample drop addition and the folding stages to integrate both devices. (E) Representation of multiplexed detection of metals showing the color development for Fe, Ni and Cu assays prior to electrochemical measurements for Zn, Cd and Pb. In (i), the labels AE, WE and RE indicate the auxiliary, working an reference electrodes, respectively. In (ii), the labels WZ, RZ and PZ indicate the waste, reaction and pre-treatment zones, respectively.

CorelDraw Graphics Suite X7™ software and cut using a Silhouette Cameo craft cutting printer (Silhouette, Belo Horizonte, MG, Brazil). The µPADs were designed in a tree-shape containing three channels with three zones each, as displayed in Fig. 1. The width and length of each channel were 1.5 and 12 mm, respectively. Three circular areas (3 mm diameter each) were integrated into each channel to be used for pretreatment zone (PZ), colorimetric detection or reaction zone (RZ) and waste zone (WZ). The bottom side of µPAD was laminated at 140 °C with a thermosensitive polyester film to avoid sample leakage. The schematic view showing the fabrication of µPADs is denoted in Fig. S1, available in the ESI.†

The ePADs were fabricated through a screen-printing process[38,39] using a conductive graphite ink containing MWCNT to enhance the analytical sensitivity.[40] To create the electrode masks, the electrode template was cut into thermosensitive polyester film using the Silhouette Cameo printer. The template was then fixed onto the vegetal paper surface and laminated at 85 °C to delimit the region in order to create the reference electrode (RE), working electrode (WE) and auxiliary electrode (AE). Then, a conductive ink composed of graphite powder, binder (vitral varnish), acetone and MWCNT was prepared, poured onto the electrode mask and spread using a spatula tool. The conductive ink was partially dried for 5 s, allowing the subsequent removal of the template mask. Afterwards, ePADs were dried to room temperature during 1 h. Finally, the pseudo reference electrode was painted with a silver ink purchased from MG Chemicals (Burlington, ON, Canada). The diameter of the working electrode was 4 mm. The protocol for manufacturing ePADs is summarized in Fig. S2, available in the ESI.†

2.3 Plug-and-play (PnP) assembling

The µPAD and ePAD were reversibly assembled using a PnP mechanism, as schematically represented in Fig. 1. A video showing in detail the assembling and the operational working in real time of the proposed dual-detection for metal analysis is represented in the ESI.†

First, a polymeric support made from thermosensitive polyester film was prepared by die cutting, as noted in Fig. 1A. The µPAD and ePAD were then fixed at the extremities of the support (Fig. 1B) and laminated at 140 °C. The coupling was achieved by folding the fixed µPAD and securing at a 45 degree angle on the support base of the ePAD. Prior to the folding step, a drop of solution was added to the ePAD surface (Fig. 1C). The µPAD was folded onto the ePAD (Fig. 1D), allowing the sample to vertically flow through the arms of the µPAD, resulting in a color change inside detection zones (Fig. 1E). After recording the colorimetric response, electrochemical measurements were then performed. Multiplexed assays were tested on assembled and integrated system aiming the simultaneous detection of heavy metals in environmental samples.

To make the device assembly robust and simple, a holder was 3D printed to promote the interface between the ePAD and the potentiostat using a USB cable. The holder was designed through the SolidWorks® 2014 software and printed by a Prusa MovtecH model open-source 3D printer (MovtecH Commercial Technology LTDA ME, São Bernado do Campo, Brazil) via fused deposition modelling employing acrylonitrile butadiene styrene as the thermoplastic filament (∅ = 1.75 mm).[41] The electrical contact was achieved using a USB
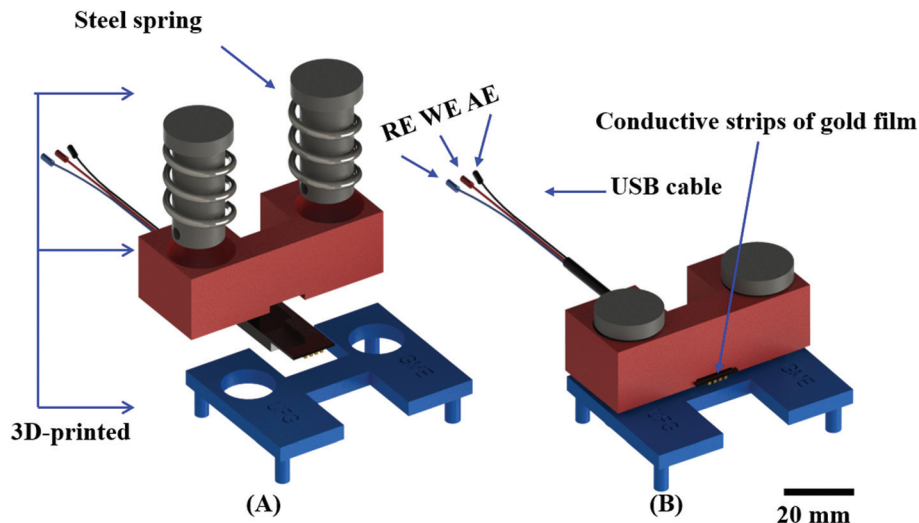
Fig. 2 (A) Representative schematic of the assembly of the 3D printed holder for electrical contact using only a USB cable, the 3D printed parts and two springs; (B) alternating cable for electrical contact of RE, WE and AE.

cable. The layout and assembly of the holder is displayed in Fig. 2. The full project in stl format is available in the ESI.†

2.4 Sample collection and preparation for analysis

To demonstrate the feasibility of the integrated device for environmental applications, four samples were collected from the Meia Ponte river located in Goiânia (Goias state, Brazil) at different locations (see Table S1 in the ESI†). The water samples were then concentrated from 100 to 10 mL on a hot plate at 100 ± 8 °C during 1 h and filtered using a nylon membrane ($\varnothing = 0.22$ μm). Afterwards, the sample was prepared in the supporting electrolyte composed of 0.1 mol L^{-1} acetate buffer and 0.1 mol L^{-1} KCl (pH = 4.5).

2.5 Simultaneous analysis

The proof-of-concept of the proposed analytical devices was demonstrated through colorimetric and electrochemical measurements. Colorimetric assays for Fe, Ni and Cu were performed using well-known protocols based on reactions with bathophenanthroline, dimethylglyoxime and bathocuproine, respectively, as described elsewhere.[9,30] For the iron assay, a 0.5 μL aliquot of hydroxylamine solution (0.1 g mL^{-1}) was added to the pretreatment zone to ensure the presence of iron in Fe(II) oxidation state. The reaction zone was sequentially spotted with aliquots (0.5 μL each) of acetate buffer (6.3 mol L^{-1}; pH = 4.5), methacrylic acid (0.7 mg mL^{-1}) and bathophenanthroline (4 mg mL^{-1}). For nickel, 0.5 μL of NaF (0.5 mol L^{-1}), and acetic acid (6.3 mol L^{-1}) was added to the pretreatment zone to mask possible interfering agents. The reaction zone was sequentially spotted with two aliquots (0.5 μL each) of ammonium hydroxide solution (pH = 9.5) and (0.5 μL each) of dimethylglyoxime (60 mmol L^{-1}). For copper, a 0.5 μL aliquot of 0.1 g mL^{-1} hydroxylamine was spotted on the pretreatment zone to promote the reduction

of Cu(II) to Cu(I). The reaction zone was sequentially spotted with aliquots (0.5 μL each) of bathocuproine (50 mg mL^{-1}), prepared in chloroform containing PEG 400 (40 mg mL^{-1}) and acetate buffer (10 mmol L^{-1}; pH = 4.5). All zones were allowed to dry for 5 min at room temperature prior to analyte addition.

For the electrochemical measurements of Zn, Cd and Pb, the working electrode surface of the ePAD was modified with bismuth (*ex situ*). Briefly, the metal was electrodeposited at the electrode surface by applying −0.9 V potential for 150 s using 100 μL of a solution containing 100 mg L^{-1} Bi(III) in acetate buffer (0.1 mol L^{-1}; pH = 4.5). Square wave anodic stripping voltammetry (SWASV) analysis was carried out by applying −1.4 V for 150 s to pre-concentrate the metals, followed by an anodic stripping step with a step potential of 5 mV, 15 mV amplitude, 15 Hz frequency, and an applied potential window from −1.4 to −0.5 V.

For the multiplexed assay on the assembled device, all reaction zones on the μPAD were pre-spotted and the working electrode was pre-modified with bismuth. A volume of 100 μL of standard or sample solution was added to the ePAD. Afterwards, the μPAD was folded onto the ePAD and kept in contact with the sample solution for 3 s. The device was then unfolded, followed by a 1 μL addition of ferricyanide solution (10 mmol L^{-1}) to the remaining solution on the electrode surface in order to mask the interference of Cu(II) during the electrochemical experiments.[44]

All colorimetric and electrochemical measurements for the detection of Cu, Fe, Ni, Zn, Cd and Pb were recorded at room temperature (25 ± 2 °C). The data obtained using the paper-based assays were compared to the results obtained using atomic absorption spectroscopy (AAS). An AAnalyst 400 spectrometer model (PerkinElmer, Waltham, MA, USA) controlled by software Syngistix™ was used.

2.6 Instrumentation

Electrochemical experiments based on SWASV and cyclic voltammetry were performed using a bipotentiostat/galvanostat model µStat 400 equipped with the DropView® software from DropSens S.L. (Oviedo, Spain). Images of the colorimetric analysis were collected using an office scanner (Hewlett-Packard, model Scanjet G4050) at a 600 dpi resolution. For the Ni and Fe assays, the images were converted to the magenta channel. The images captured for the Cu assay were converted to yellow channel. The color intensity was extracted using a region of interest (ROI) defined with 3 mm diameter. For all colorimetric measurements, the pixel intensity was analyzed using the Corel Photo-Paint™ software.

3. Results and discussion

Electrochemical and colorimetric detection modes have been independently coupled to paper-based analytical devices for a variety of applications.[9,31] The coupling of both electrochemical and colorimetric detection techniques on the same platform could prove to be a powerful analytical tool for multiplexed analysis in paper-based devices. Aiming for the best performance of both detection modes, the composition of the conductive electrode material, the type of the paper used for fabricating ePAD and µPAD as well as the electrochemical and colorimetric parameters were thoroughly investigated and the results are presented in the ESI (see Fig. S3–S10 and Tables S2–S5†). In summary, the best electrochemical response was achieved a mixture of graphite, binder and MWCNT at ratio of $150:150:12$ (in mass) on vegetal paper. The morphological characterization based on scanning electron microscopy revealed well-defined graphite particles impregnated with MWCNT on paper surface. For fabricating the µPAD, the best performance was obtained when using a tree-shape channel design printed on chromatography paper. It is important to emphasize that the present manufacturing process employed a home cutter printer (~US$ 300) to create microfluidic channels, colorimetric reactions zones and electrodes. The cost of the integrated device comprising both µPAD and ePAD was estimated to be *ca*. U$ 0.03 (see summarized details in Table S6, available in the ESI†).

3.1 3D printed holder to assemble ePADs and the integrated device

We next sought to integrate the detection modes into a single device using a vertical folding mechanism. Considering the high cost of the commercial electrical cables needed to connect the electrodes and the potentiostat, an external holder was developed first. The 3D printed components were designed to enable simple and reproducible assembly of the colorimetric µPAD and the ePAD. One component of the holder allows for the assembly of the ePAD *via* vertical pressure between two plates, with one plate containing 3 conductive strips (gold film), as presented in Fig. 2. Unlike commercially available standard cables, the 3D printed alternative system promotes the fitting of electrochemical sensors defined at different thickness (0.5 to 5 mm), without damage to the conductive tracks. To demonstrate the feasibility of the proposed 3D printed system, a cyclic voltammogram using a redox probe composed of 5.0 mmol L^{-1} [Fe (CN)$_6$]$^{4-/3-}$ in 0.1 mol L^{-1} KCl was collected and compared to data obtained using a commercial cable. As displayed in Fig. S11,† both cables revealed similar performance. Considering the recorded peak current signal, the percentual difference was lower than 3%. Fig. 3 displays a visual representation of the integration of the ePAD and µPAD using the 3D printed holder.

3.2 Performance of the vertical folding

The vertical folding mechanism is a key factor in properly integrating the colorimetric and electrochemical detection modes through PnP strategy, allowing for multiplexed analysis of several analytes in the same sample. The µPADs and ePADs were fabricated independently and then fixed to the polymeric support. The design of the coupling mechanism is flexible to allow an easy and reversible assembly of the two independent paper-based sensors unlike previous examples where the coupling was fixed. To demonstrate the performance of the inte-
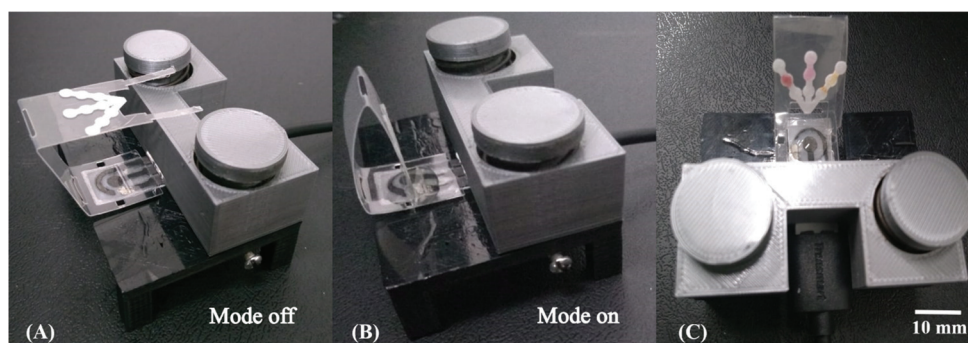

Fig. 3 Schematic view of the 3D printed holder integrating both µPAD and ePAD through vertical folding assembly. Images (A) and (B) show the assembling of the multiplexed device before (mode off) and after (mode on) coupling, respectively. Image (C) depicts the disconnected µPAD after colorimetric assays enabling the use of ePAD for metal analysis using the same sample aliquot.

grated device, colorimetric and electrochemical measurements were performed on the devices with and without the coupling mechanism. For this purpose, the experiments without the coupling mechanism were performed using ePADs in the static mode and the µPADs under common lateral flow assays. The effect of the vertical coupling mechanism for both electrochemical and colorimetric assays was evaluated using a model solution containing Zn(II), Cd(II) and Pb(II) (1000 µg L^{-1} each) and Fe(II), Ni(II) and Cu(II) (5 mg L^{-1} each). The results are presented in Fig. 4.

For the colorimetric results presented in Fig. 4A, it can be noted that the color intensities for all analytes with and without coupling are quite similar. Comparing the data before and after coupling, the differences in color intensity for Fe, Ni and Cu ranged from 3.4 to 4.4%. These results indicate that the vertical and reversible foldable coupling mechanism does not compromise the analytical performance of the colorimetric assays. For the SWASV experiments, the current values were also compared before and after coupling between the µPAD and ePAD. As can be seen in Fig. 4B, the current values after coupling were slightly higher than the those prior to assembly. On average, the differences in the signal response before and after coupling ranged between 11 and 15%. For each device, the results of the assays before and after coupling were compared. The calculated t values (2.53 for µPADs and −2.52 for ePADs) were lower than the critical t value (2.91), thus demonstrating no statistical difference (p = 0.05). These results prove that the PnP strategy does not interfere on the analytical performance of colorimetric and electrochemical assays performed independently.

In addition, the PnP coupling has allowed the dual colorimetric/electrochemical detection using the same aliquot of sample. This is advantageous over independent devices since they require different sample aliquots to promote colorimetric/electrochemical measurements. In comparison with independent devices, the PnP mechanism has promoted the detection

of multiple metals in a shorter period of time with satisfactory performance.

As already stated, Rattanarat *et al.*[26] reported the development of a multilayer sensor based on an assembly *via* horizontal folding using double-sided adhesive tape. The approach described by the authors resulted in an irreversible coupling, thus hindering the use of steps associated to the removal of interfering metals (like Cu) on electrochemical measurements and compromising the control of the aspirated sample volume by capillary action during the colorimetric lateral flow assays on µPADs. In the novel integration mechanism proposed herein, assays were first performed on the µPAD to avoid common problems associated to the sample evaporation. This versatility was ensured due to the reversible integration, which enabled the simple connection and disconnection of both µPAD and ePAD based on PnP mechanism. Furthermore, it is important to note that electrochemical measurements were conducted in the presence of ferricyanide solution to mask possible copper interferences.[44] Using this strategy, no interference from ferricyanide was observed because the redox process occurs at higher potentials. Since ferricyanide exhibits a yellowish color, the presence of ferricyanide solution could promote an interference on the colorimetric response. To avoid any possible contamination, electrochemical assays were carried out after disconnecting the µPAD from the integrated system. The sequential analysis ensures the proper analytical performance of both the µPAD and ePAD, which aims the multiplexed analysis of several metals for routine on site analysis of environmentally relevant compounds.

3.3 Analytical performance

The analytical performance of the integrated device was investigated to demonstrate its environmental feasibility. The linear concentration ranges and the limits of detection for Zn(II), Cd(II), Pb(II), Fe(II), Ni(II) and Cu(II) ions were evaluated in
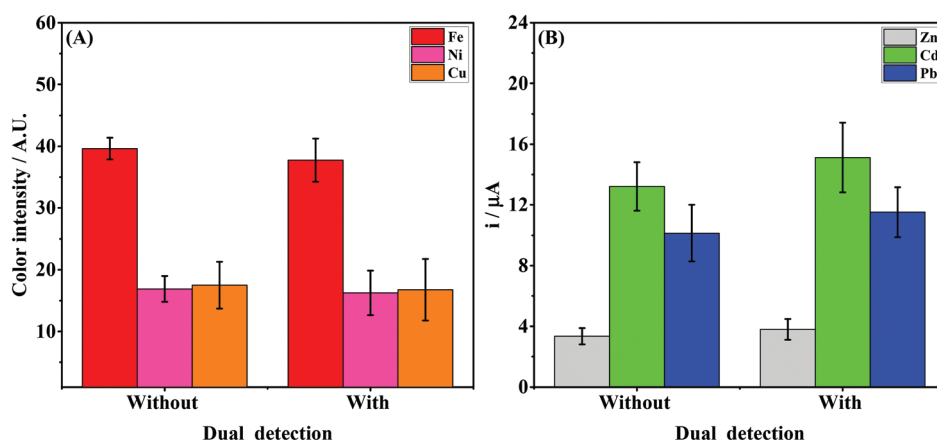

Fig. 4 Representation of the data for the (A) colorimetric assay for Fe(II), Ni(II) and Cu(II) (5 mg L^{-1} each) and (B) SWASV experiments for Zn(II), Cd(II) and Pb(II) (1000 µg L^{-1} each) with and without the vertical sliding coupling mechanism. The colored columns and error bars indicate the average response and standard deviation values, respectively (n = 3). SWASV conditions: −1.4 V for 150 s (preconcentration stage), 5 mV step potential, 15 mV amplitude, 5 Hz frequency, and potential window from −1.4 to −0.5 V.
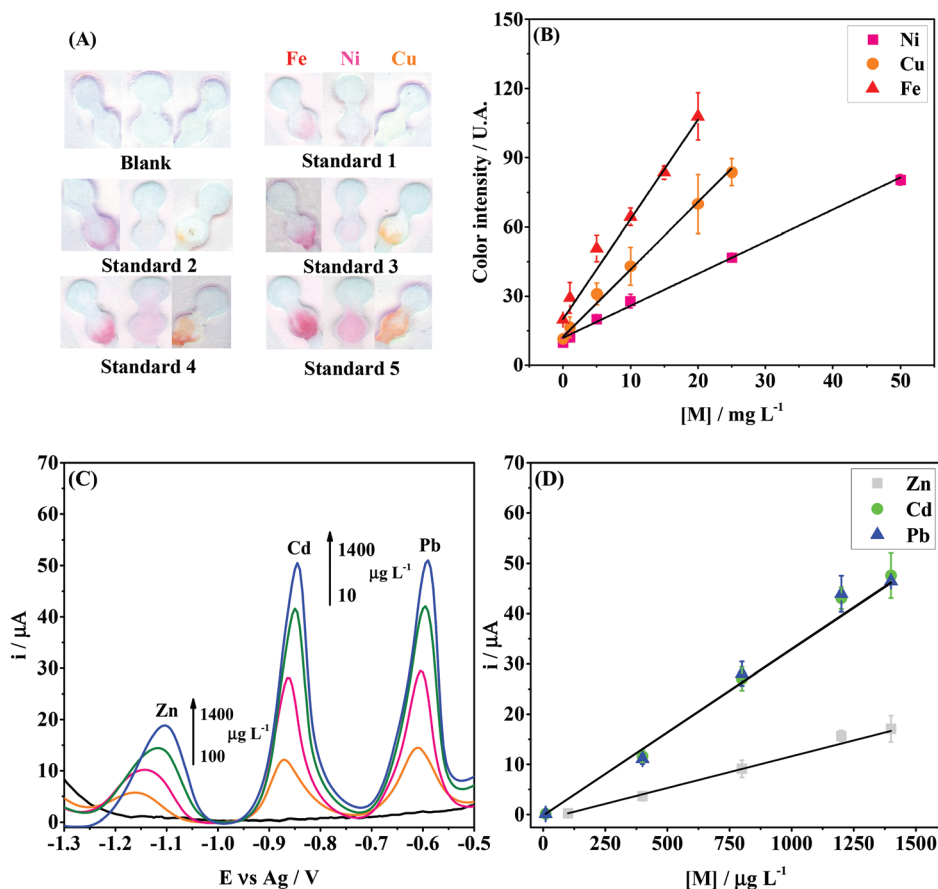
Fig. 5 Colorimetric and electrochemical performance of the integrated paper-based device for the multiplexed analysis of metals. (A) Scanned images after colorimetry assays for Fe(II), Ni(II) and Cu(II) at different concentrations; (B) calibration curves for Fe, Ni and Cu, with the following regression equations: $y_{Fe} = (20 \pm 3) + (4.3 \pm 0.2)[Fe]$, $y_{Ni} = (11.9 \pm 0.7) + (1.39 \pm 0.03)[Ni]$ and $y_{Cu} = (12 \pm 1) + (2.92 \pm 0.09)[Cu]$; (C) SWASV results for Zn(II), Cd(II), Pb(II) at different concentrations; (D) calibration curves for Zn, Cd and Pb with the following regression equations: $y_{Zn} = (-1.02 \pm 0.05) + (0.0126 \pm 0.0005)[Zn]$, $y_{Cd} = (-0.17 \pm 0.02) + (0.033 \pm 0.001)[Cd]$ and $y_{Pb} = (-0.196 \pm 0.04) + (0.0332 \pm 0.0004)[Pb]$. In graphs (B) and (D), the points and error bars indicate the average response and standard deviation values, respectively, for three measurements each. SWASV conditions: The same from those used in Fig. 4, except the frequency (15 Hz).

acetate buffer (0.1 mol L^{-1}; pH = 4.5) while keeping all previously optimized conditions constant.

The colorimetric assays for Fe(II), Ni(II) and Cu(II) revealed linear behavior ($R^2 > 0.99$) in the concentration ranges of 1–20 mg L^{-1}, 1–50 mg L^{-1} and 1–25 mg L^{-1}, respectively. Fig. 5A and B display the digital images and calibration curves, respectively. The limit of detection (LOD) values obtained for Fe(II), Ni(II) and Cu(II) were 0.1, 0.3 and 0.2 mg L^{-1}, respectively. The LODs were calculated based on the ratio between three times the standard deviation obtained for the blank and the slope of the calibration curve. The assays for Zn, Cd and Pb were performed by SWASV and the peak current signals are denoted in Fig. 5C. A linear behavior ($R^2 > 0.99$) was observed in the concentration ranges from 100 to 1400 µg L^{-1} for Zn(II), and 10 to 1400 µg L^{-1} for Cd(II) and Pb(II), as seen in Fig. 5D. The LOD values calculated for Zn(II), Cd(II) and Pb(II) were 10.5, 1.3 and 0.9 µg L^{-1}, respectively. The results were compared to other reports found in the literature and are summarized in Table 1.

In comparison to other reports found in the literature, the analytical platform with dual detection proposed herein has offered new attractive features, as can be seen in the summary presented in Table 1. For the electrochemical measurements, the linear concentration range was wider than previous reports. The LODs obtained for electrochemical analysis of Zn, Cd and Pb were similar to those described using other electrochemical paper-based sensors.[10] Regarding the colorimetric assays for Fe, Ni and Cu, it is important to mention that the linear concentration range and the LOD values were similar to other reports showing colorimetric approaches only.[9,16] On the other hand, considering the simultaneous electrochemical and colorimetric assays, the analytical performance of the proposed device was better than that reported by Rattanarat et al.[26] As noted in Table 1, the use of a folding mechanism offered linear response in a lower concentration range and better LOD values for Fe, Ni and Cu. To the best of our knowledge, this is the first study showing the reversible coupling of µPAD and ePAD via a vertical folding mechanism, allowing

Table 1 Comparison of analytical performance for Fe, Ni, Cu, Zn, Cd, and Pb detection to other studies with different analytical platforms

| | Linear concentration range and (LOD) | | | | | | |
| | Colorimetric | | | SWASV | | | |
Analytical platform	Fe	Ni (mg L^{-1})	Cu	Zn	Cd (µg L^{-1})	Pb	Ref.
Glass	—	—	—	0.5–11 (0.23)	0.5–11 (0.07)	0.5–11 (0.18)	43
Ceramic	—	—	—	0.1–100 (0.09)	0.1–100 (0.06)	0.1–100 (0.08)	33
Plastic	—	—	—	5–400 (5.0)	0.5–400 (0.5)	0.1–500 (0.1)	44
Plastic	—	—	—	—	1–200 (0.2)	1–200 (0.3)	34
Paper	—	15–60 (4.8)	5–80 (1.6)	—	—	—	45
Paper/plastic	30–300 (15)	30–300 (15)	60–300 (15)	—	5–150 (1.0)	5–150 (1.0)	26
Paper	1–20 (0.25)	1–20 (0.40)	1–20 (0.50)	—	—	—	9
Paper	—	—	—	5–40 (1.1)	5–40 (0.9)	—	10
Paper	0.3–18 (0.20)	0.4–23 (0.30)	0.05–24 (0.03)	—	—	—	16
Paper	1–20 (0.1)	1–50 (0.3)	1–25 (0.2)	100–1400 (10.5)	10–1400 (1.3)	10–1400 (0.9)	This study

suitable performance for multiplexed analysis of six metals in environmental samples. It is important to emphasize that the LOD values achieved for all metals are enough to allow the detection of these analytes in river water samples according to US Environmental Protection Agency.[1,42]

The reproducibility of the colorimetric and electrochemical devices was investigated (Fig. S12†). For the vertical flow assays performed on five µPADs, the relative standard deviation (RSD) ranged from 4.6 to 13.8%. Similarly, the reproducibility of ePADs (*n* = 5) was evaluated through SWASV experiments and the achieved RSD values for the peak current varied from 3.9 to 8.4%. Thereby, the proposed method for integrating a µPAD and ePAD through the PnP mechanism has offered excellent linearity in a wide concentration range for SWASV experiments, good sensitivity for both the electrochemical and colorimetric assays in comparison to other studies,[42,43] and it revealed suitable reproducibility for the multiplexed detection of six metals.

3.4 Interference study

Several other metals present in the environmental samples can potentially interfere with both the colorimetric and electrochemical measurements due to competing complexation with the chromogens and stripping during SWASV analysis, respectively.[4,9,42] For this reason, the selectivity of the integrated device was evaluated in the presence of potential interfering agents. As mentioned in the Experimental section, pretreatment zones were added in the device design to minimize possible interfering of other metals on the colorimetric response. The analytical response in the absence and presence of potential interferences at different tolerance ratios is displayed in Fig. 6. As it can be seen, the Mn(II), Al(III), Sb(II), Ba (II), Cd(II), Zn(II), Pb(II), Ni(II) and Fe(II) ions did not significantly interfere on the SWASV analysis of Zn, Cd and Pb. However, Cu(II) ions interfered on Zn, Cd and Pb detection at tolerance ratios of 2, 5 and 5, respectively. To minimize Cu(II) inferences, ferricyanide was added to the sample solution during SWASV.[44]

Calorimetrically, the Mn(II), Sb(II), Zn(II) and Pb(II) ions did not interfere on the observed color intensity. On the other
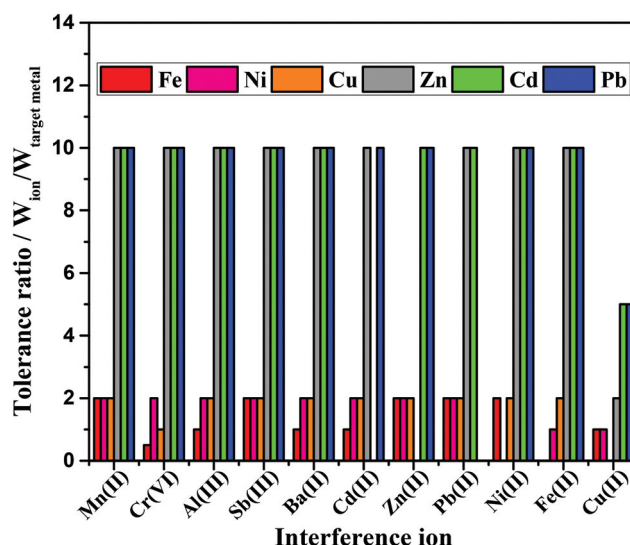
Fig. 6 Tolerance ratio of heavy metal detection considering the interference ion ≤10%, using target metals solutions of 500 µg L^{-1} for Zn(II), Cd(II), Pb(II) and 5.0 mg L^{-1} for Fe(II), Ni(II), Cu(II).

hand, Al(III), Ba(II), Cd(II), Fe(II) and Cu(II) ions demonstrated to be potential interfering agents on the multiplexed colorimetric detection interfered with detection within the tolerance ratio equal to 1 (interference ≤10%). In addition, Cr(VI) ion revealed a most pronounced inference on the Fe detection (tolerance ratio 0.5).

3.5 Multiplex detection of metals in river water samples

The method herein proposed was explored for the multiplexed detection of metals in river water samples collected at four different sites along the Meia Ponte river's course. The sampling sites included 2 locations prior to the waste treatment station (WTS) and 2 locations after the WTS. The concentrations of the metals observed at all sites are displayed in Fig. 7. It is important to emphasize that Zn and Ni were not detected in any of the collected samples. Interestingly, Fe, Cd and Pb were found in the sample collected at the site #1 at
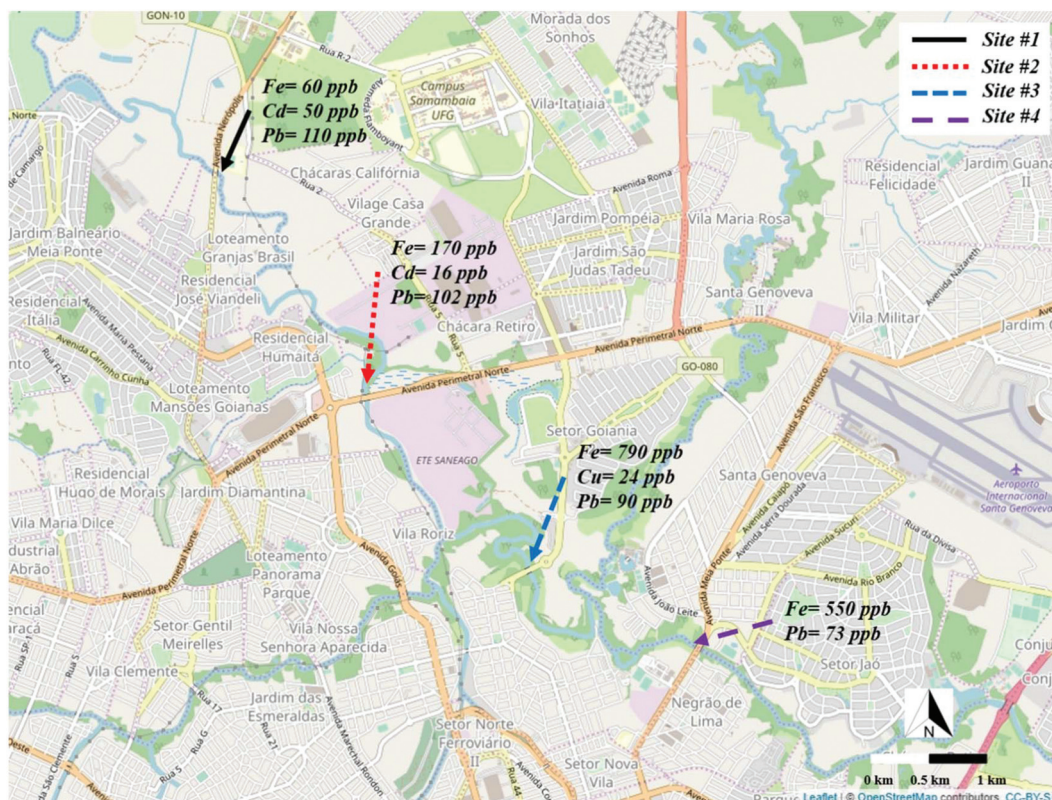
Fig. 7 Representation of the sampling sites on the Meia Ponte river and the respective heavy metals concentrations.

concentrations of 60 ± 5, 50 ± 4, and 110 ± 8 µg L^{-1}, respectively. For the sample collected at the 2nd location, the concentrations for Fe, Cd and Pb were 170 ± 11, 16 ± 1, and 102 ± 9 µg L^{-1}, respectively. For the site #3, which was located after the WTS, Fe, Cu and Pb were detected at concentrations of 790 ± 19, 24 ± 5 and 90 ± 12 µg L^{-1}, respectively. For the 4th location, Fe and Pb were found in concentrations around 550 ± 33 and 73 ± 10 µg L^{-1}, respectively.

Based on the data presented, it can be seen that the Fe concentration considerably increased in the sites located after the WTS. This increase may be associated with the use of ferric chloride as coagulant in the WTS to promote the precipitation of the organic material.[46] In addition, the presence of Cu was observed at the site #3, which is indicative of contamination in the river likely caused by the improper treatment of the waste. A decrease in the Cd concentration was noted across the sites #1 and #2 and the absence of this metal was observed after the WTS. Lastly, a slight decrease in the Pb concentration was observed from 112 ± 8 to 73 ± 10 µg L^{-1} along the river course. This behavior is similar to that of Cd and it may be related to bioavailability of the metals.[47,48]

The accuracy of the proposed method was investigated through recovery experiments by spiking the sample with standard solutions of Fe, Ni and Cu (2 mg L^{-1} each) and Zn, Cd and Pb (200 µg L^{-1} each). Based on the recorded data, the recovery values ranged from 76.5 to 121.1%, as summarized in

Table 2 Comparison of the metal concentrations found in water samples using the proposed multiplexed device and the AAS technique ($n = 3$)

Metal	Found concentration (mg L^{-1})	
	AAS	Proposed method
Zn	0.97 ± 0.01	0.7 ± 0.1
Cd	1.14 ± 0.01	1.2 ± 0.2
Pb	1.12 ± 0.04	0.9 ± 0.1
Fe	1.64 ± 0.03	1.6 ± 0.1
Ni	4.95 ± 0.03	6.0 ± 0.6
Cu	3.35 ± 0.03	3.4 ± 0.4

Table S7, available in the ESI.† Additionally, the reliability of the method was compared to a reference technique (atomic absorption spectrometry) and the obtained data are presented in Table 2. As it can be noted, the metal concentrations found using the multiplexed device revealed good agreement with the data obtained through AAS technique.

The results achieved by both methodologies were compared to each other through a paired t-test. The calculated t value ($t = -0.58$) was below the critical t value ($t = 2.01$), and it can be concluded that the reference and experimental data sets did not statistically differ from each other at the 95% confidence level.

4. Conclusions

In summary, this report has described for the first time a simple "plug-and-play" strategy to integrate paper-based colorimetric and electrochemical devices. The novel coupling mechanism minimized effects associated to sample evaporation and ensured no sample loss. The integrated device revealed great feasibility for multiplexed analysis of Zn, Cd, Pb, Fe, Ni and Cu. The proof-of-concept aiming environmental application was successfully demonstrated through the detection of metals in river water samples collected in four different points. The achieved concentrations varied from 16 to 786 $\mu g\ L^{-1}$ the proposed approach did not present statistical difference from the results recorded through atomic absorption spectrometry, thus revealing accuracy and reliability for routine analysis. Although an offline preconcentration stage has been performed to demonstrate the proof-of-concept using environmental samples, future efforts will be devoted to promote the integration of this analytical step on the same platform, making it simpler and faster for on-site applications. Based on the data presented in this study, we believe that the multiplexed device coupled with dual detection can emerge as a powerful, portable and disposable tool for monitoring environmental pollutants. Lastly, it is important to highlight that the integrated device was fully fabricated on paper-based platforms and integrated using a polyester substrate (transparency), thus offering the possibility to be developed in any place with limited resources exploiting low cost and globally affordable consumables.

Author contributions

Habdias A. Silva-Neto: conceptualization, investigation, methodology, validation, writing – original draft. Thiago M. G. Cardoso: investigation, writing – original draft preparation. Catherine J. McMahon: investigation, validation, writing – review & editing. Lívia F. Sgobbi: investigation, resources, writing – original draft preparation. Charles S. Henry: conceptualization, supervision, writing – reviewing and editing. Wendell K. T. Coltro: conceptualization, funding acquisition, supervision, writing – reviewing and editing.

Conflicts of interest

There are no conflicts of interest to declare.

Acknowledgements

References

1 A. Gałuszka, Z. M. Migaszewski and J. Namieśnik, *Environ. Res.*, 2015, **140**, 593–603.

2 R. Das, C. D. Vecitis, A. Schulze, B. Cao, A. F. Ismail, X. Lu, J. Chen and S. Ramakrishna, *Chem. Soc. Rev.*, 2017, **46**, 6946–7020.

3 X. Liu, Y. Yao, Y. Ying and J. Ping, *TrAC, Trends Anal. Chem.*, 2019, **115**, 187–202.

4 Y. Lin, D. Gritsenko, S. Feng, Y. C. Teh, X. Lu and J. Xu, *Biosens. Bioelectron.*, 2016, **83**, 256–266.

5 W. Zhang, S. Zhu, R. Luque, S. Han, L. Hu and G. Xu, *Chem. Soc. Rev.*, 2016, **45**, 715–752.

6 H. A. Silva-Neto, T. M. G. Cardoso, W. K. T. Coltro and R. C. Urban, *Anal. Methods*, 2019, **11**, 4861–4952.

7 E. Noviana, C. P. McCord, K. M. Clark, I. Jang and C. S. Henry, *Lab Chip*, 2020, **20**, 9–34.

8 E. Carrilho, A. W. Martinez and G. M. Whitesides, *Anal. Chem.*, 2009, **81**, 7091–7095.

9 L. Zhang, L. Guan, Z. Lu, M. Li, J. Wu, R. Cao and J. Tian, *Talanta*, 2019, **196**, 408–414.

10 C. Kokkinos, A. Economou and D. Giokas, *Sens. Actuators, B*, 2018, **260**, 223–226.

11 D. M. Cate, J. A. Adkins, J. Mettakoonpitak and C. S. Henry, *Anal. Chem.*, 2015, **87**, 19–41.

12 W. R. de Araujo, T. M. G. Cardoso, R. G. da Rocha, M. H. P. Santana, R. A. A. Muñoz, E. M. Richter, T. R. L. C. Paixão and W. K. T. Coltro, *Anal. Chim. Acta*, 2018, **1034**, 1–21.

13 G. Hernandez-Vargas, J. E. Sosa-Hernández, S. Saldarriaga-Hernandez, A. M. Villalba-Rodríguez, R. Parra-Saldivar and H. M. N. Iqbal, *Biosensors*, 2018, **8**, 1–21.

14 K. Yamada, T. G. Henares, K. Suzuki and D. Citterio, *Angew. Chem., Int. Ed.*, 2015, **54**, 5294–5310.

15 S. R. Chinnadayyala, J. Park, H. T. N. Le, M. Santhosh, A. N. Kadam and S. Cho, *Biosens. Bioelectron.*, 2019, **126**, 68–81.

16 F. Li, Y. Hu, Z. Li, J. Liu, L. Guo and J. He, *Anal. Bioanal. Chem.*, 2019, **411**, 6497–6508.

17 K. Yamada, D. Citterio and C. S. Henry, *Lab Chip*, 2018, **18**, 1485–1493.

18 L. A. Pradela-filho, D. A. G. Araújo, R. M. Takeuchi and A. L. Santos, *Electrochim. Acta*, 2017, **258**, 786–792.

19 C. L. S. Chagas, F. R. De Souza, T. M. G. Cardoso, R. C. Moreira, J. A. F. Da Silva, D. P. De Jesus and W. K. T. Coltro, *Anal. Methods*, 2016, **8**, 6682–6686.

20 M. Li, R. Cao, A. Nilghaz, L. Guan, X. Zhang and W. Shen, *Anal. Chem.*, 2015, **87**, 2555–2559.

21 M. Santhiago, M. Strauss, M. P. Pereira, A. S. Chagas and C. C. B. Bufon, *ACS Appl. Mater. Interfaces*, 2017, **9**, 11959–11966.

22 N. Dossi, R. Toniolo, A. Pizzariello, F. Impellizzieri, E. Piccin and G. Bontempelli, *Electrophoresis*, 2013, **34**, 2085–2091.

23 J. G. Giuliani, T. E. Benavidez, G. M. Duran, E. Vinogradova, A. Rios and C. D. Garcia, *J. Electroanal. Chem.*, 2016, **765**, 8–15.

24 T. Cho and J. Wang, *Electroanalysis*, 2018, **30**, 1028–1032.

25 W. R. de Araujo, C. M. R. Frasson, W. A. Ameku, J. R. Silva, L. Angnes and T. R. L. C. Paixão, *Angew. Chem., Int. Ed.*, 2017, **56**, 15113–15117.

26 P. Rattanarat, W. Dungchai, D. Cate, J. Volckens, O. Chailapakul and C. S. Henry, *Anal. Chem.*, 2014, **86**, 3555–3562.

27 N. A. Meredith, C. Quinn, D. M. Cate, T. H. Reilly, J. Volckens and C. S. Henry, *Analyst*, 2016, **141**, 1874–1887.

28 S. Li, C. Zhang, S. Wang, Q. Liu, H. Feng, X. Ma and J. Guo, *Analyst*, 2018, **143**, 4230–4246.

29 B. Gao, X. Li, Y. Yang, J. Chu and B. He, *Analyst*, 2019, **144**, 6497–6511.

30 J. P. Devadhasan and J. Kim, *Sens. Actuators, B*, 2018, **273**, 18–24.

31 J. Mettakoonpitak, J. Volckens and C. S. Henry, *Anal. Chem.*, 2020, **92**, 1439–1446.

32 H. Wang, L. Yang, S. Chu, B. Liu, Q. Zhang, L. Zou, S. Yu and C. Jiang, *Anal. Chem.*, 2019, **91**, 9292–9299.

33 S. Chaiyo, E. Mehmeti, K. Žagar, W. Siangproh, O. Chailapakul and K. Kalcher, *Anal. Chim. Acta*, 2016, **918**, 26–34.

34 D. Martín-Yerga, I. Álvarez-Martos, M. C. Blanco-López, C. S. Henry and M. T. Fernández-Abedul, *Anal. Chim. Acta*, 2017, **981**, 24–33.

35 T. G. Silva, W. R. De Araujo, R. A. A. Muñoz, E. M. Richter, M. H. P. Santana, W. K. T. Coltro and T. R. L. C. Paixão, *Anal. Chem.*, 2016, **88**, 5145–5151.

36 A. Apilux, W. Dungchai, W. Siangproh, N. Praphairaksit, C. S. Henry and O. Chailapakul, *Anal. Chem.*, 2010, **82**, 1727–1732.

37 S. Chaiyo, A. Apiluk, W. Siangproh and O. Chailapakul, *Sens. Actuators, B*, 2016, **233**, 540–549.

38 T. R. de Oliveira, W. T. Fonseca, G. de Oliveira Setti and R. C. Faria, *Talanta*, 2019, **195**, 480–489.

39 L. A. Pradela-Filho, I. A. A. Andreotti, J. H. S. Carvalho, D. A. G. Araújo, L. O. Orzari, A. Gatti, R. M. Takeuchi, A. L. Santos and B. C. Janegitz, *Sens. Actuators, B*, 2019, 127433.

40 Y. Sameenoi, M. M. Mensack, K. Boonsong, R. Ewing, W. Dungchai, O. Chailapakul, D. M. Cropek and C. S. Henry, *Analyst*, 2011, **136**, 3177–3184.

41 A. A. Dias, C. L. S. Chagas, H. A. Silva-Neto, E. O. Lobo-Junior, L. F. Sgobbi, W. R. de Araujo, T. R. L. C. Paixão and W. K. T. Coltro, *ACS Appl. Mater. Interfaces*, 2019, **11**, 34484–39492.

42 S. Li, C. Zhang, S. Wang, Q. Liu, H. Feng, X. Ma and J. Guo, *Analyst*, 2018, **143**, 4230–4246.

43 N. M. Thanh, N. Van Hop, N. D. Luyen, N. H. Phong and T. T. T. Toan, *Adv. Mater. Sci. Eng.*, 2019, **2019**, 1826148.

44 J. Mettakoonpitak, J. Mehaffy, J. Volckens and C. S. Henry, *Electroanalysis*, 2017, **29**, 880–889.

45 X. Sun, B. Li, A. Qi, C. Tian, J. Han, Y. Shi, B. Lin and L. Chen, *Talanta*, 2018, **178**, 426–431.

46 G. A. O. Jian-yang, G. A. O. Fang-zhou and Z. H. U. Feng, *J. Cent. South Univ.*, 2019, **26**, 449–457.

47 J. De Anda, M. S. Gradilla-hernández and O. Díaz-torres, *Environ. Monit. Assess.*, 2019, **191**, 1–13.

48 J. Dong, X. Xia, Z. Zhang, Z. Liu, X. Zhang and H. Li, *J. Environ. Sci.*, 2018, **74**, 79–87.